JCI The Journal of Clinical Investigation

Dystrophins carrying spectrin-like repeats 16 and 17 anchor nNOS to the sarcolemma and enhance exercise performance in a mouse model of muscular dystrophy

Yi Lai, … , Ronald L. Terjung, Dongsheng Duan

J Clin Invest. 2009;119(3):624-635. https://doi.org/10.1172/JCI36612.

Research Article

Sarcolemma-associated neuronal NOS (nNOS) plays a critical role in normal muscle physiology. In Duchenne muscular dystrophy (DMD), the loss of sarcolemmal nNOS leads to functional ischemia and muscle damage; however, the mechanism of nNOS subcellular localization remains incompletely understood. According to the prevailing model, nNOS is recruited to the sarcolemma by syntrophin, and in DMD this localization is altered. Intriguingly, the presence of syntrophin on the membrane does not always restore sarcolemmal nNOS. Thus, we wished to determine whether dystrophin functions in subcellular localization of nNOS and which regions may be necessary. Using in vivo transfection of dystrophin deletion constructs, we show that sarcolemmal targeting of nNOS was dependent on the spectrin-like repeats 16 and 17 (R16/17) within the rod domain. Treatment of *mdx* mice (a DMD model) with R16/17-containing synthetic dystrophin genes effectively ameliorated histological muscle pathology and improved muscle strength as well as exercise performance. Furthermore, sarcolemma-targeted nNOS attenuated α-adrenergic vasoconstriction in contracting muscle and improved muscle perfusion during exercise as measured by Doppler and microsphere circulation. In summary, we have identified the dystrophin spectrin-like repeats 16 and 17 as a novel scaffold for nNOS sarcolemmal targeting. These data suggest that muscular dystrophy gene therapies based on R16/17-containing dystrophins may yield better clinical outcomes than the current therapies.

 Related Commentary, page 448

Dystrophins carrying spectrin-like repeats 16 and 17 anchor nNOS to the sarcolemma and enhance exercise performance in a mouse model of muscular dystrophy

Yi Lai,[1] Gail D. Thomas,[2] Yongping Yue,[1] Hsiao T. Yang,[3] Dejia Li,[1] Chun Long,[1] Luke Judge,[4] Brian Bostick,[1] Jeffrey S. Chamberlain,[4] Ronald L. Terjung,[3] and Dongsheng Duan[1]

[1]Department of Molecular Microbiology and Immunology, School of Medicine, University of Missouri, Columbia, Missouri, USA. [2]Hypertension Division, University of Texas Southwestern Medical Center, Dallas, Texas, USA. [3]Department of Biomedical Sciences, College of Veterinary Medicine, University of Missouri, Columbia, Missouri, USA. [4]Department of Neurology, University of Washington, Seattle, Washington, USA.

Sarcolemma-associated neuronal NOS (nNOS) plays a critical role in normal muscle physiology. In Duchenne muscular dystrophy (DMD), the loss of sarcolemmal nNOS leads to functional ischemia and muscle damage; however, the mechanism of nNOS subcellular localization remains incompletely understood. According to the prevailing model, nNOS is recruited to the sarcolemma by syntrophin, and in DMD this localization is altered. Intriguingly, the presence of syntrophin on the membrane does not always restore sarcolemmal nNOS. Thus, we wished to determine whether dystrophin functions in subcellular localization of nNOS and which regions may be necessary. Using in vivo transfection of dystrophin deletion constructs, we show that sarcolemmal targeting of nNOS was dependent on the spectrin-like repeats 16 and 17 (R16/17) within the rod domain. Treatment of *mdx* mice (a DMD model) with R16/17-containing synthetic dystrophin genes effectively ameliorated histological muscle pathology and improved muscle strength as well as exercise performance. Furthermore, sarcolemma-targeted nNOS attenuated α-adrenergic vasoconstriction in contracting muscle and improved muscle perfusion during exercise as measured by Doppler and microsphere circulation. In summary, we have identified the dystrophin spectrin-like repeats 16 and 17 as a novel scaffold for nNOS sarcolemmal targeting. These data suggest that muscular dystrophy gene therapies based on R16/17-containing dystrophins may yield better clinical outcomes than the current therapies.

Introduction

Neuronal NOS (nNOS) plays critical roles in a variety of muscle activities, including contraction, regeneration, atrophy, glucose uptake, and blood perfusion (1). In normal skeletal muscle, nNOS is localized to the cytosolic surface of the sarcolemma. This position is critical for nNOS function. During muscle contraction, activated nNOS produces NO. The membrane location of nNOS allows ready diffusion of NO to the muscle vasculature. Consequently, vessels are dilated to meet the increased metabolic needs of contracting muscle (2, 3).

Duchenne muscular dystrophy (DMD) is caused by dystrophin deficiency (4). Despite the fact that dystrophin is missing in all myofibers, muscle disease does not occur simultaneously throughout the entire muscle. The characteristic early histopathology in DMD muscle closely resembles focal necrosis seen after functional ischemia (5, 6). The identification of nNOS as a component of the dystrophin-associated glycoprotein complex (DGC) provides a molecular explanation for the unique muscle lesions in DMD (7, 8). In the absence of dystrophin, the entire DGC (including nNOS) fails to assemble at the sarcolemma. Delocalization of nNOS impairs compensatory vasodilation during muscle contraction and subsequently leads to focal ischemia and necrosis (2, 3). For similar reasons, Duchenne patients are more easily fatigued than normal people (9, 10).

The mechanism(s) by which nNOS is recruited to the sarcolemma are not completely understood. According to the prevailing model, nNOS is brought to the sarcolemma by the scaffolding protein syntrophin. Several lines of evidence support this model. First, syntrophin itself is recruited to the sarcolemma by a syntrophin-binding motif in the dystrophin C-terminal domain (11–13). In the absence of the dystrophin C-terminal domain, syntrophin can still be recruited to the sarcolemma by dystrobrevin, possibly through the sarcoglycan complex (14–16). Second, syntrophin forms a complex with nNOS through a noncanonical interaction between PDZ (postsynaptic density 95, discs large, and zonula occludens–1) and PDZ domain (7, 8, 17, 18). Finally, genetic ablation of the syntrophin gene or the PDZ domain of the syntrophin gene eliminates sarcolemmal nNOS (19, 20).

Despite the compelling evidence, this model cannot explain all the existing data. Most intriguingly, the presence of syntrophin on the membrane does not always lead to sarcolemmal nNOS expression. This was first demonstrated in Becker muscular dystrophy (BMD), a milder allelic form of DMD (21). Synthetic mini-/microdystrophin genes that have been developed for DMD gene therapy

Conflict of interest: The authors have declared that no conflict of interest exists.

Nonstandard abbreviations used: AAV, adeno-associated virus; BMD, Becker muscular dystrophy; BL10, C57BL/10; C, dystrophin C-terminal domain; CK, creatine kinase; DGC, dystrophin-associated glycoprotein complex; DMD, Duchenne muscular dystrophy; EDL, extensor digitorum longus; H, hinge region in the dystrophin rod domain; nNOS, neuronal NOS; PDZ, postsynaptic density 95, discs large, and zonula occludens–1; R, dystrophin spectrin-like repeat; TA, tibialis anterior.

Citation for this article: *J. Clin. Invest.* **119**:624–635 (2009). doi:10.1172/JCI36612.

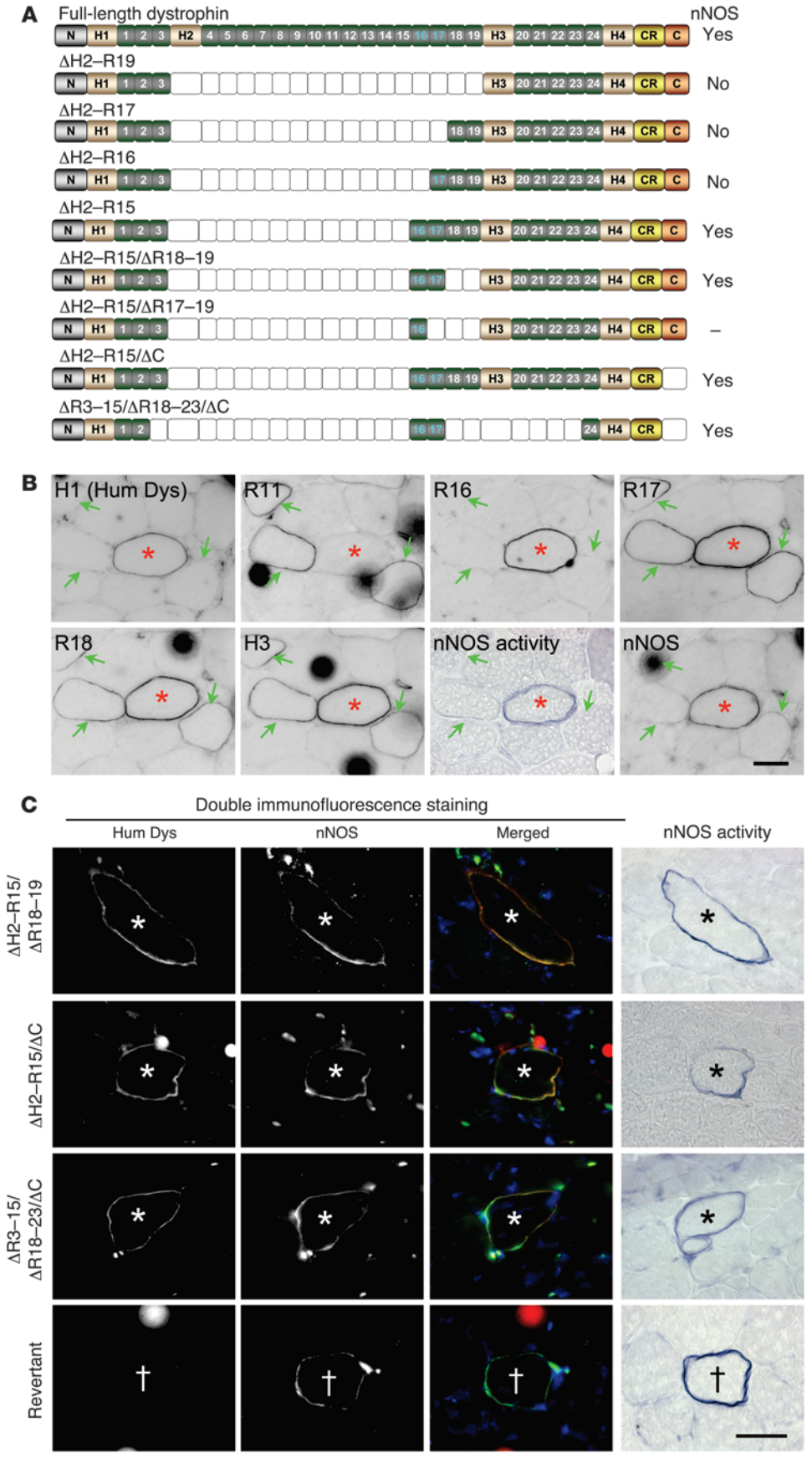

Figure 1
Sarcolemmal nNOS localization depends on the rod, but not the C-terminal, domain of dystrophin. (**A**) Schematic outline of the full-length and synthetic dystrophin constructs. "Yes" indicates that nNOS is recruited to the sarcolemma by the construct; "No" indicates that the construct cannot restore nNOS to the sarcolemma. Dotted boxes denote deleted regions. (**B**) The ΔH2–R15 minidystrophin anchors nNOS to the sarcolemma. Representative photomicrographs of dystrophin immunostaining, nNOS activity staining, and nNOS immunostaining in the ΔH2–R15 minigene plasmid–transfected *mdx* muscle. Dystrophin was revealed by epitope-specific antibodies (H1, R11, R16, R17, R18, and H3). The H1 antibody only recognizes human dystrophin (Hum Dys). Other dystrophin antibodies recognize both human and mouse dystrophin. Asterisks indicate a minigene-transfected myofiber; arrows, revertant myofibers. Scale bar: 20 μm. (**C**) Sarcolemmal nNOS localization does not require the C-terminal domain, nor is it dependent on the repeats adjacent to R16/17. Representative photomicrographs of human dystrophin/nNOS double immunostaining and nNOS activity staining on serial sections from the ΔH2–R15/ΔR18–19, ΔH2–R15/ΔC, and ΔR3–15/ΔR18–23/ΔC plasmid–transfected *mdx* muscles. Asterisks indicate dystrophin plasmid–transfected fibers; crosses, revertant myofibers. Scale bar: 50 μm.

Table 1
Sarcolemmal nNOS expression in dystrophin plasmid–transfected *mdx* muscle

Construct	*n*[A]	Immunostaining-positive myofibers			nNOS activity–positive myofibers	nNOS restoration efficiency[C]
		Hum Dys$^+$/nNOS$^+$	Hum Dys$^+$/nNOS$^-$	Hum Dys$^-$/nNOS$^+$[B]		
Full-length	9	89	1[D]	5	94	98.89%
No plasmid	8	0	0	8	8	–
ΔH2–R19	8	0	73	6	6	0.00%
ΔH2–R17	10	0	83	4	4	0.00%
ΔH2–R16	8	0	72	4	4	0.00%
ΔH2–R15	6	45	1[D]	6	51	97.83%
ΔH2–R15/ΔR18–19	3	15	0	4	19	100.00%
ΔH2–R15/ΔR17–19	8	0	0	7	7	–
ΔH2–R15/ΔC	3	8	0	4	12	100.00%
ΔR3–15/ΔR18–23/ΔC	3	5	0	2	7	100.00%

[A]Sample size (the number of muscles examined). [B]These are revertant myofibers. [C]nNOS restoration efficiency was calculated as (nNOS and human dystrophin double-positive fibers)/(human dystrophin–positive fibers). [D]Human dystrophin (Hum Dys) staining is faint in these fibers. This may be due to low expression levels or examination of the end of a positive fiber.

also fail to anchor nNOS to the sarcolemma, although they are able to restore syntrophin (16, 22, 23). In addition, the dissociation between syntrophin and nNOS expression was observed in α-dystrobrevin–knockout mice (24). In these mice, the absence of α-dystrobrevin barely affects the syntrophin level, but nNOS is substantially reduced (24). Collectively, these results suggest a ternary interaction model for nNOS localization. Here, we hypothesized that in addition to a direct interaction between syntrophin and nNOS, one and/or multiple regions of dystrophin might have also contributed to nNOS localization by either directly interacting or indirectly stabilizing the syntrophin–nNOS complex.

To test this hypothesis, we generated a series of synthetic dystrophin genes and evaluated nNOS restoration by in vivo plasmid transfection, AAV-mediated gene transfer, and generation of a transgenic mouse model. After confirming dystrophin expression with a panel of epitope-specific antibodies, we examined nNOS expression by single and double immunostaining, in situ nNOS activity assay, and Western blot analysis. More than half of the dystrophin gene (from exon 3 to exon 52) has been implicated in nNOS localization (21). Surprisingly, we found that only a fairly small region in the middle of the dystrophin rod domain (R16 and R17, abbreviated as R16/17 herein) was required. Yeast two-hybrid assay results suggested that nNOS localization might be mediated by a coordinated effort of both R16/17 and the syntrophin PDZ domain, although the latter displayed a higher affinity for the nNOS PDZ domain. Based on these results, we developed several R16/17-containing mini- and microdystrophin genes as potential candidate genes for DMD/BMD gene therapy. In vivo studies in mouse models of DMD suggest that these newly developed candidate genes were as effective as the previously published mini- and microgenes in mitigating dystrophic histopathology and improving muscle force. In contrast to the previous candidate genes, the newly developed genes also restored sarcolemmal nNOS. In hemodynamic, tissue blood flow, and treadmill assays, R16/17-containing dystrophin significantly improved perfusion in contracting muscle and enhanced exercise performance.

Results

Dystrophin recruits nNOS to the sarcolemma through the rod, not the C-terminal, domain. The full-length dystrophin gene can recruit nNOS to the sarcolemma, but the ΔH2–R19 minigene cannot (Figure 1 and Table 1) (23, 25). The ΔH2–R19 minigene has the same structure as the full-length gene, except for a large deletion in the rod domain. The deletion represents approximately 48% of the dystrophin coding sequence and includes 1 hinge (H2) and 16 spectrin-like repeats (from R4 to R19). To localize the nNOS recruiting domain, we gradually added back the deleted region to the human ΔH2–R19 minigene and evaluated the nNOS recruiting capacity (Figure 1, Table 1, and Supplemental Figures 1–3; supplemental material available online with this article; doi:10.1172/JCI36612DS1).

Transfected myofibers were identified with a human dystrophin H1–specific antibody. nNOS expression was confirmed on serial sections by immunostaining and in situ nNOS activity assay. Sarcolemmal nNOS expression was not restored when R18/19 or R17/18/19 were inserted back into the ΔH2–R19 minigene (Table 1 and Supplemental Figures 2 and 3). However, restoring 4 repeats (R16/17/18/19) recovered sarcolemmal nNOS expression (Figure 1B, Table 1, and Supplemental Figure 2).

To determine whether all 4 added repeats contributed to nNOS restoration, we deleted R18/19 or R17/18/19 from the ΔH2–R15 minigene (Figure 1A). Removing R18/19 did not affect sarcolemmal nNOS expression (Figure 1C and Table 1). For unknown reasons, we were unable to detect ΔH2–R15/ΔR17–19 minigene expression in transfected *mdx* muscle (Figure 1A and Table 1).

Next, we evaluated the contribution of the dystrophin C-terminal domain. This domain has been suggested to indirectly facilitate nNOS recruitment by bringing syntrophin to the sarcolemma (11–13). However, when the C-terminal domain was deleted from the full-length gene, there was minimal impact on sarcolemmal nNOS expression (15). Consistent with this previous report, when the C-terminal domain was deleted from the ΔH2–R15 minigene, we did not detect any change in nNOS localization either (Figure 1C and Table 1). Together, these results suggest that the C-terminal domain is not required for nNOS recruitment in either the full-length gene or the abbreviated minigenes.

All 3 nNOS-recruiting minigenes (ΔH2–R15, ΔH2–R15/ΔR18–19, and ΔH2–R15/ΔC) shared 2 common features. They all contained a rod domain longer than that of the ΔH2–R19 minigene, and they all carried R16/17 with R16 flanked by R3. To determine whether the length of the rod domain and the configuration of the flanking repeats are important for nNOS recruitment, we generated the

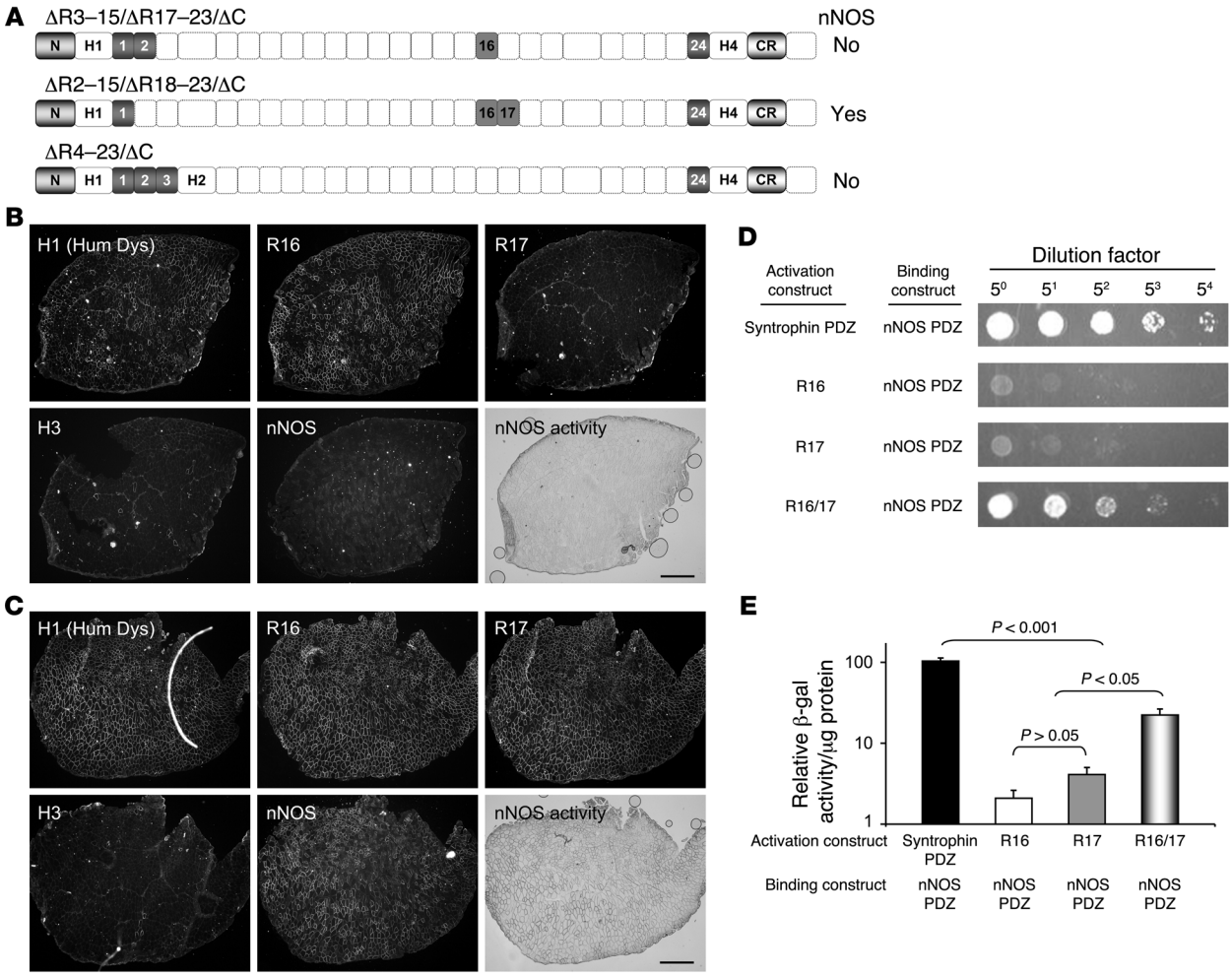

Figure 2

Both R16 and R17 are indispensable for sarcolemmal nNOS localization. (**A**) Schematic outline of the microdystrophin constructs. "Yes" indicates that nNOS is recruited to the sarcolemma by the construct; "No" indicates that nNOS is not recruited. Dotted boxes denote deleted regions. (**B** and **C**) Both R16 and R17 are required for sarcolemmal nNOS localization. Representative serial immunostaining and nNOS activity staining photomicrographs of *mdx* muscles infected with AV.CMV.ΔR3–15/ΔR17–23/ΔC (**B**) or AV.CMV.ΔR2–15/ΔR18–23/ΔC (**C**). Sarcolemmal nNOS localization was observed only in microdystrophin carrying both R16 and R17 (**C**) but not in microdystrophin carrying only R16 (**B**). Scale bars: 500 μm. See Supplemental Figure 4 for high-magnification images. (**D**) Representative yeast two-hybrid assay results (from 5 independent experiments) reveal interaction between R16/17 and the nNOS PDZ domain. Individual repeat R16 alone or R17 alone does not bind the nNOS PDZ domain. (**E**) Relative β-galactosidase activity from the quantitative yeast two-hybrid assay. $n = 6$ for each group.

ΔR3–15/ΔR18–23/ΔC microgene. This microgene contains only 5 repeats. Furthermore, R16 is flanked by R2. Despite a much smaller rod domain and different flanking repeats, sarcolemmal nNOS expression was restored by the ΔR3–15/ΔR18–23/ΔC microgene (Figure 1C and Table 1).

In summary, our results suggest that R16/17 is crucial for dystrophin-mediated nNOS recruitment. Furthermore, the nNOS recruiting activity is independent of the C-terminal domain and independent of the neighboring repeats adjacent to R16/17.

nNOS localization requires both R16 and R17. The findings from the ΔH2–R16 construct suggest that the presence of R17 alone is not sufficient to recruit nNOS (Figure 1A, Table 1, Supplemental Figure 2, and Supplemental Figure 3D). Since we did not observe expression from the ΔH2–R15/ΔR17–19 minigene, it was not clear whether R16 by itself was sufficient for nNOS recruitment.

To address this issue, we generated 2 microdystrophin constructs. Both have 4 repeats in the rod domain. However, one contained only R16 (ΔR3–15/ΔR17–23/ΔC) and the other contained both R16 and R17 (ΔR2–15/ΔR18–23/ΔC) (Figure 2A). After packaging these constructs into adeno-associated virus 6 (AAV-6) vectors, we delivered them to the tibialis anterior (TA) muscles of 50-day-old *mdx* mice. At 30 days after AAV infection, we examined microgene and nNOS expression (Figure 2, A–C, and Supplemental Figure 4). We observed efficient transduction from both vectors (≥90%) (Figure 2, B and C). However, only the construct containing R16/17 (ΔR2–15/ΔR18–23/ΔC) restored sarcolemmal nNOS (Figure 2C and Supplemental Figure 4). These data strongly suggest that nNOS recruitment requires both R16 and R17 and that either one alone is not sufficient.

R16/17 interacts with the nNOS PDZ domain. To further understand the contribution of R16/17 to nNOS recruiting, we per-

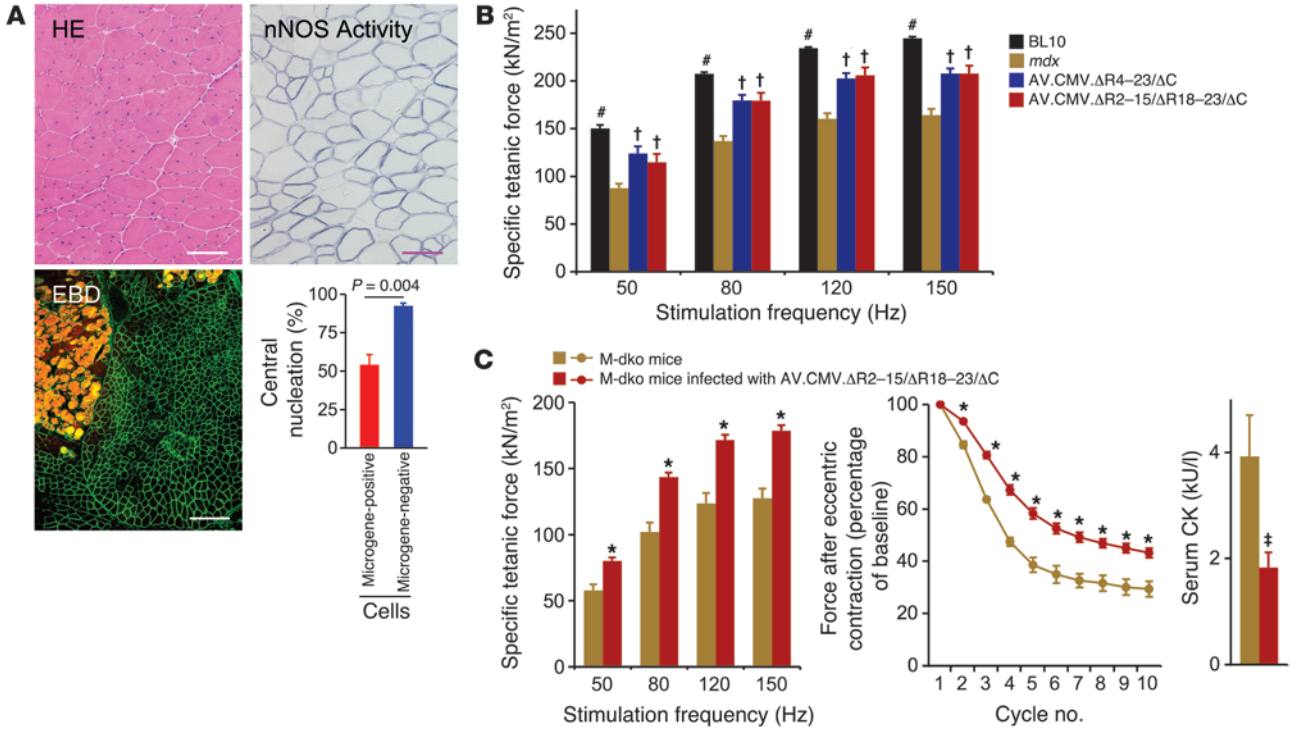

Figure 3
The R16/17-containing microgene ameliorates muscle disease and improves muscle force following AAV gene transfer. (**A**) Results from adult *mdx* muscle (local delivery; $n = 4$–8 for each assay). Top: Serial sections with H&E and nNOS activity staining (see immunostaining in Supplemental Figure 5); scale bar: 100 μm. Bottom left: Evans blue dye (EBD) uptake; scale bar: 400 μm. An R16-specific antibody revealed the microgene. Bottom right: Central nuclear quantification. (**B**) Specific tetanic force in the *mdx* EDL muscle following systemic neonatal microgene therapy. $^{\#}P \le 0.033$ compared with all other groups; $^{\dagger}P \le 0.001$ compared with *mdx* only. (**C**) Systemic delivery of AV.CMV.ΔR2–15/ΔR18–23/ΔC to adult MyoD/dystrophin double-knockout (M-dko) mice improved skeletal muscle function and reduced the serum CK level. Sample size for muscle function assay: $n = 4$ for uninfected littermate controls; $n = 14$ for AV.CMV.ΔR2–15/ΔR18–23/ΔC–infected mice. Sample size for the CK assay: $n = 3$ for uninfected littermate controls; $n = 6$ for AV.CMV.ΔR2–15/ΔR18–23/ΔC–infected mice. $^{*}P \le 0.002$, $^{\ddagger}P = 0.015$ compared with controls.

formed a yeast two-hybrid assay (Figure 2, D and E). We cloned the nNOS PDZ domain into a binding construct. We also generated a series of the activation constructs carrying R16, R17, or R16/17. As a positive control, we also made an activation construct containing the syntrophin PDZ domain. Interaction with the nNOS PDZ domain was observed with R16/17 and the syntrophin PDZ domain, but not with R16 or R17 alone (Figure 2D). Similar results were obtained when the nNOS PDZ domain was cloned into the activation constructs, and other components (R16, R17, R16/17, or the syntrophin PDZ domain) were cloned into the binding constructs (data not shown). To compare the relative binding affinity for the nNOS PDZ domain, we performed a quantitative yeast two-hybrid assay (Figure 2E). Despite an absolute requirement of R16/17 for nNOS localization (Figures 1 and 2), the binding affinity between R16/17 and the nNOS PDZ domain was 5-fold lower than that between the syntrophin PDZ domain and the nNOS PDZ domain. Taken together, these results suggest that dystrophin R16/17 may assist sarcolemmal nNOS localization by interacting with the nNOS PDZ domain.

The R16/17-containing microgene ameliorates dystrophic pathology and improves muscle strength in mouse models for DMD. An important goal of this study is to improve current AAV-mediated DMD gene therapy. We have already demonstrated that an R16/17-containing microgene, ΔR2–15/ΔR18–23/ΔC, can restore sarcolemma nNOS (Figure 2 and Supplemental Figure 4). However, it is not clear whether this microgene can ameliorate dystrophic pathology. It is known that some microgenes cannot mitigate muscle disease (26).

To address this issue, we delivered AAV-6 AV.CMV.ΔR2–15/ΔR18–23/ΔC to the gastrocnemius muscle of 2-month-old *mdx* mice. The sarcolemmal integrity and central nucleation were examined at 40 and 60 days after gene transfer, respectively (transduction efficiency was ~80%). Expressing the ΔR2–15/ΔR18–23/ΔC microgene efficiently prevented sarcolemmal leakage, as evidenced by the lack of Evans blue dye accumulation in transduced myofibers (Figure 3A). The percentage of central nucleation reflects pathogenic muscle degeneration/regeneration. We observed a significant reduction in central nucleation in the ΔR2–15/ΔR18–23/ΔC microgene–positive myofibers (Figure 3A and Supplemental Figure 5).

Next, we examined muscle strength. We have previously established the ΔR4–23/ΔC microgene as the best candidate microgene (16, 26, 27). Here we compared muscle force in ΔR4–23/ΔC and ΔR2–15/ΔR18–23/ΔC microgene–treated *mdx* mice. We delivered AAV-9 AV.CMV.ΔR4–23/ΔC or AV.CMV.ΔR2–15/ΔR18–23/ΔC to newborn *mdx* mice through facial vein injection. At 3 months after systemic gene transfer, we examined microgene expression and muscle force in the extensor digitorum longus (EDL) muscle (Figure 3B). Consistent with our previous reports (28), we observed

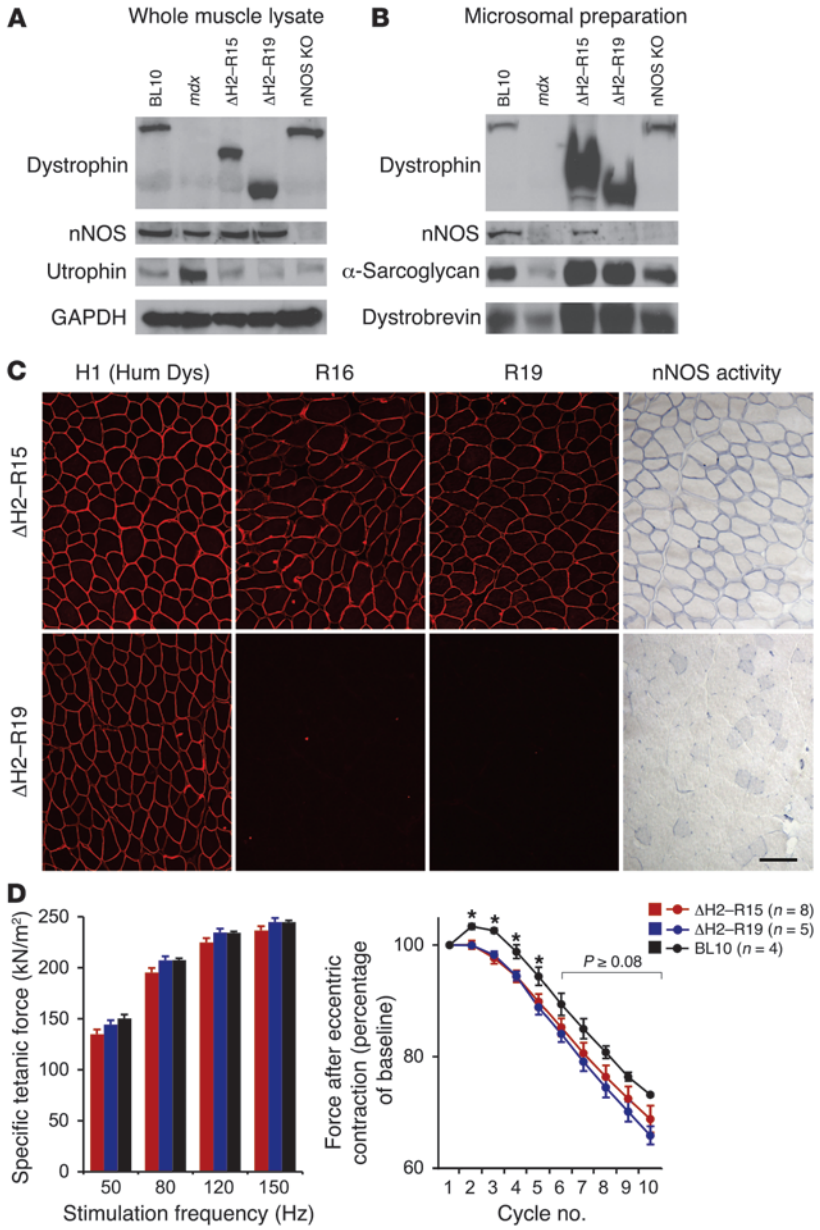

Figure 4
The R16/17-containing minigene (ΔH2–R15) restores sarcolemmal nNOS, normalizes muscle force to wild-type levels, and reduces eccentric contraction–associated muscle injury. (**A**) Representative Western blots of whole muscle lysates from the TA muscles of BL10, *mdx*, ΔH2–R15 transgenic *mdx*, ΔH2–R19 transgenic *mdx*, and nNOS-knockout mice. GAPDH was used as the loading control. (**B**) Representative Western blots of microsomal preparations from the quadriceps femoris muscles. (**C**) Representative photomicrographs of dystrophin immunostaining (H1, R16, R19) and nNOS activity staining from ΔH2–R15 and ΔH2–R19 transgenic *mdx* mice. Scale bar: 100 μm. (**D**) The ΔH2–R15 minigene normalizes muscle-specific force and prevents eccentric contraction-induced injury. $^*P \leq 0.021$ compared with transgenic *mdx* mice.

highly efficient gene transfer with both AAV vectors (~80%, data not shown). Muscle force was also significantly enhanced by both microgenes (Figure 3B). Importantly, the extent of force improvement was identical.

To further evaluate the therapeutic effect of the ΔR2–15/ΔR18–23/ΔC microgene, we performed systemic AAV delivery in *mdx4cv* mice. This model carries a different mutation in the dystrophin gene, and it is on a different genetic background (C57BL/6 rather than C57BL/10 [BL10]). Consistent with our findings in *mdx* mice, AV.CMV.ΔR2–15/ΔR18–23/ΔC significantly increased limb muscle strength and reduced serum creatine kinase (CK) levels in *mdx4cv* mice (Supplemental Figure 6).

In contrast to those in human patients, the clinical manifestations are quite mild in both *mdx* and *mdx4cv* mice. This is partially due to robust muscle regeneration. MyoD is a master transcription regulator for skeletal muscle differentiation. Eliminating MyoD abolishes muscle regeneration in *mdx* mice. As a result, MyoD-null *mdx* mice develop a more severe skeletal muscle disease that better models the human condition (29). To validate the therapeutic efficacy of the ΔR2–15/ΔR18–23/ΔC microgene in a symptomatic model, we delivered AAV-9 AV.CMV.ΔR2–15/ΔR18–23/ΔC to 2-month-old MyoD-null *mdx* mice through tail vein injection. Three months after systemic gene transfer, the EDL muscle specific force was significantly enhanced in AAV-treated mice (Figure 3C). Furthermore, eccentric contraction–induced muscle injury was mitigated, and serum CK levels were significantly reduced (Figure 3C). Taken together, the results indicate that the R16/17-containing microgene AAV vector recovered sarcolemmal nNOS and ameliorated muscle pathology.

The R16/17-containing minigene improves vascular perfusion in contracting muscle and enhances exercise performance. The minigenes are 60%–80% larger than the microgenes, and they yield better functional recovery in *mdx* mice (25, 26). However, none of the current minigenes contain R16/17, nor can they restore nNOS. Here, we tested whether adding R16/17 could further improve the therapeutic efficacy of the minigene. We generated ΔH2–R15 and ΔH2–R19 minigene transgenic *mdx* and *mdx4cv* mice (Figures 4–7 and Supplemental Figures 7, 8, and 10). The ΔH2–R15 minigene carries R16/17, but the ΔH2–R19 minigene does not (Figure 1 and Table 1).

On Western blot analysis, we observed minidystrophin bands of the expected size (Figure 4A). nNOS was detected in whole muscle lysate from both ΔH2–R19 and ΔH2–R15 transgenic mice (Figure 4A). However, in membrane-enriched microsomal preparation, it was detected only in ΔH2–R15 transgenic mice (Figure 4B). Immunofluorescence staining and in situ nNOS activity staining further confirmed Western blot results (Figure 4C). These studies revealed human minigene expression in both transgenic strains. The ΔH2–R15 transgenic mice also expressed R16, -17, -18, and -19, four repeats that were missing in ΔH2–R19 transgenic mice (Figure 4C; data not shown for R17 and R18 immunostaining). Importantly, nNOS expression and nNOS activity were only detected in

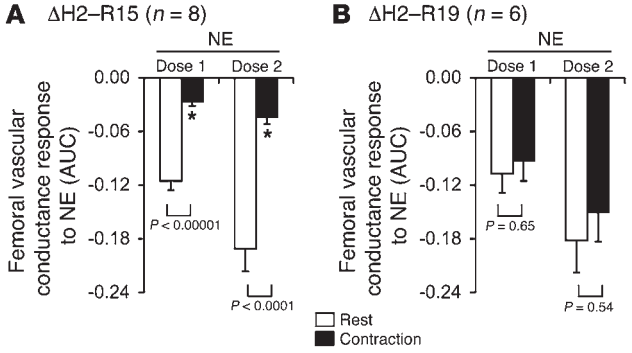

Figure 5
The ΔH2–R15 minigene attenuates norepinephrine-mediated vasoconstriction in contracting muscle. Decreases in femoral vascular conductance were recorded following intraarterial injection of 2 doses of norepinephrine (NE) into the resting and contracting hind limbs of male HSA(human skeletal α-actin promoter).ΔH2–R15 and HSA.ΔH2–R19 transgenic *mdx* mice. (**A**) Results from ΔH2–R15 transgenic *mdx* mice. (**B**) Results from ΔH2–R19 transgenic *mdx* mice. AUC is presented in arbitrary units. Asterisks indicate significant differences.

muscle sections from ΔH2–R15 transgenic mice (Figure 4C; data not shown for nNOS immunostaining).

Muscle-specific force was completely restored to wild-type levels in both ΔH2–R19 and ΔH2–R15 minigene transgenic mice (Figure 4D) (26). When challenged with eccentric contraction, the 2 types of transgenic mice showed identical responses (Figure 4D). In the first 4 cycles, the force preservation was slightly lower than that in BL10 mice. From the fifth to the tenth cycle, there were no significant differences among the 3 groups (Figure 4D).

A critical function of membrane-associated nNOS is to generate NO to counteract α-adrenergic vasoconstriction during muscle contraction. The loss of this protective mechanism leads to functional ischemia and thus aggravates contraction-induced injury in dystrophin-deficient muscles (2, 3, 30). To determine whether the restoration of sarcolemmal nNOS by the R16/17-containing minigene could improve blood perfusion during muscle contraction, we compared femoral vascular conductance in ΔH2–R15 and ΔH2–R19 transgenic *mdx* and *mdx4cv* mice (Figure 5 and Supplemental Figures 7 and 8) (2). In resting muscle, the 2 strains displayed similar femoral vascular conductance (data not shown). When resting muscles were challenged with norepinephrine, the strains also showed similar reductions in femoral artery conductance (Figure 5 and Supplemental Figure 8). However, we observed a striking difference in contracting muscle. In ΔH2–R19 transgenic mice and transgene-negative littermates from ΔH2–R15 breeding, norepinephrine-induced vasoconstriction was not attenuated in the contracting muscles (Figure 5 and Supplemental Figure 7). In contrast, in ΔH2–R15 transgenic mice, the constrictor response provoked by norepinephrine administration was significantly reduced in the contracting muscles (Figure 5 and Supplemental Figure 8).

To further explore muscle perfusion in the intact animal, we directly measured blood flow using radiolabeled microspheres. We observed similar levels of kidney perfusion in ΔH2–R15 and ΔH2–R19 transgenic mice, irrespective of the activity status (resting or exercising) (Figure 6). The two strains also showed similar muscle perfusion at rest (Figure 6A). However, ΔH2–R15 transgenic mice demonstrated significantly greater muscle perfusion during the treadmill exercise (Figure 6B).

To measure the physiological benefit of nNOS restoration, we developed a treadmill protocol. Since muscle perfusion in sarcolemmal nNOS-deficient mice was compromised (Figure 5, Figure 6, and Supplemental Figures 7 and 8), we hypothesized that intensive daily exercise would lead to muscle ischemia in these mice. We further hypothesized that the accumulation of ischemic damage would reduce running performance at later time points. As expected, BL10 mice showed a gradual increase in running distance up to 10 days with daily exercise (the duration of the study), while the running distance of *mdx* mice leveled off after day 4 (Supplemental Figure 9). Although this finding supports our hypothesis, we cannot rule out the possibility that the inherent muscle pathology might have limited treadmill performance in *mdx* mice.

To exclude the potential influence of muscle disease, we next compared running performance in ΔH2–R15 and ΔH2–R19 transgenic *mdx* mice under a similar treadmill exercise regimen. We have shown that both ΔH2–R15 and ΔH2–R19 minigenes can efficiently ameliorate muscle pathology and improve muscle contraction (Figure 3A and Figure 4D) (25, 26). In this case, should we observe distinctive performance profiles, it would be more likely

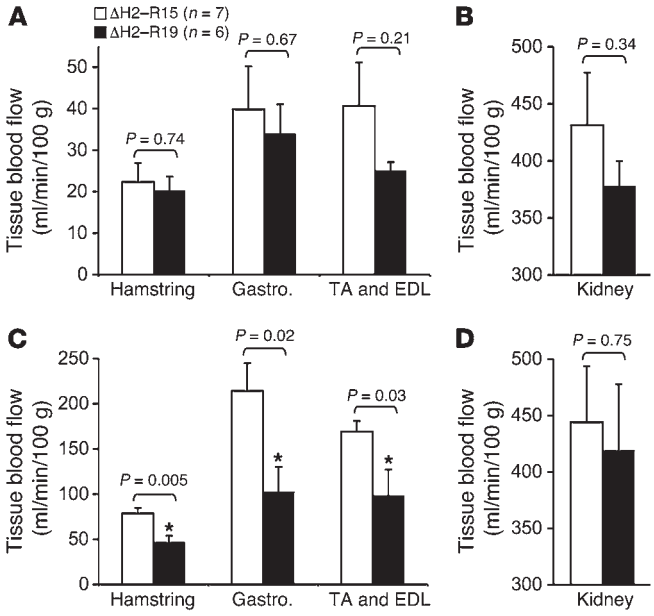

Figure 6
The ΔH2–R15 minigene transgenic *mdx* mice show better muscle perfusion during exercise. Muscle and internal organ perfusion at rest and during exercise was quantified using radiolabeled microspheres in male HSA.ΔH2–R15 and HSA.ΔH2–R19 transgenic *mdx* mice. (**A**) Tissue perfusion in selected muscles at rest. (**B**) Kidney perfusion at rest. (**C**) Tissue perfusion in selected muscles during exercise. (**D**) Kidney perfusion during exercise. Gastro., gastrocnemius muscle. Asterisks indicate significant differences.

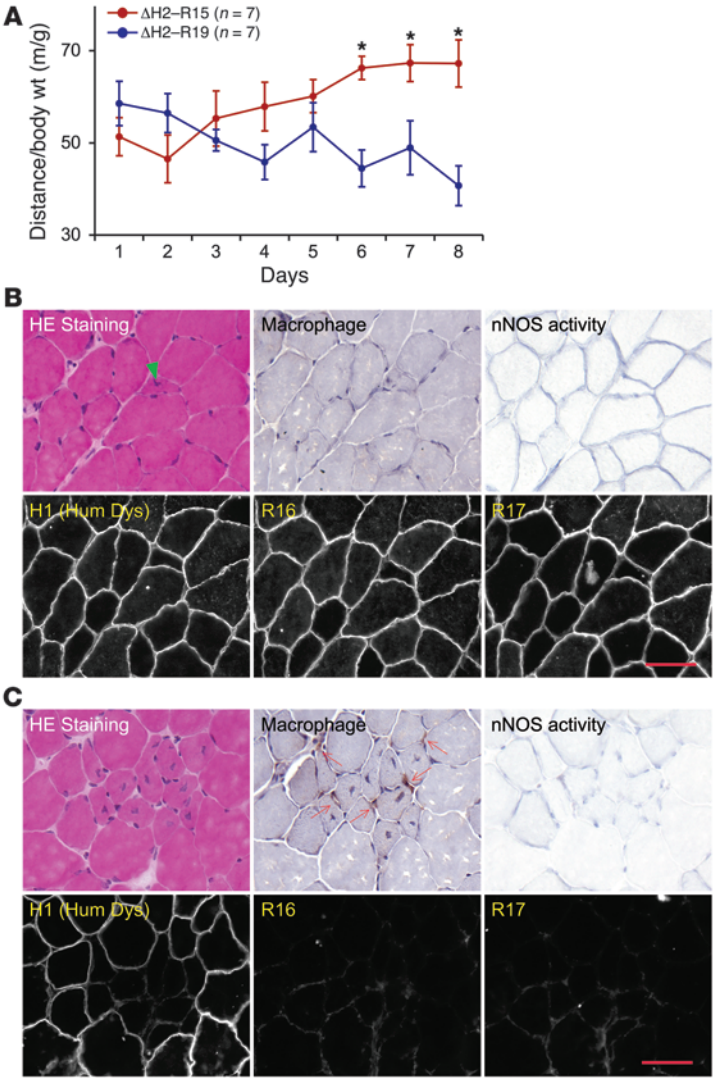

Figure 7
The ΔH2–R15 minigene prevents ischemic injury and enhances performance during intensive exercise. (**A**) Body weight–normalized daily running distance in HSA.ΔH2–R15 and HSA.ΔH2–R19 transgenic *mdx* mice (6-month-old male mice). *$P \leq 0.02$. (**B** and **C**) Representative photomicrographs of general histopathology (H&E staining), inflammation (macrophage infiltration), nNOS activity, and minidystrophin expression (immunostaining with epitope-specific antibodies) in the limb muscle harvested after 8 days' intensive treadmill running. (**B**) Results from ΔH2–R15 transgenic *mdx* mice. Arrowhead indicates a single regenerating myofiber. (**C**) Results from ΔH2–R19 transgenic *mdx* mice. Arrows indicate macrophages. Scale bars: 50 μm. See Supplemental Figure 10 for low-magnification images.

due to the difference in sarcolemmal nNOS localization between the 2 strains. Consistent with our hypothesis, treadmill performance was gradually improved in ΔH2–R15, but not in ΔH2–R19, transgenic *mdx* mice (Figure 7A). Starting from day 6, ΔH2–R19 transgenic *mdx* mice showed significantly shorter running distances than ΔH2–R15 transgenic *mdx* mice (Figure 7A). Our observation in ΔH2–R19 transgenic *mdx* mice was further confirmed in ΔR4–23 transgenic *mdx* mice (Supplemental Figure 9). Similar to the ΔH2–R19 minigene, the ΔR4–23 microgene cannot restore sarcolemmal nNOS. These mice showed a running profile similar to that of *mdx* mice (Supplemental Figure 9). Additional studies revealed less than 1% human dystrophin expression in the heart of all transgenic *mdx* mice (data not shown). Hence, the difference in exercise performance is unlikely due to accidental cardiac rescue.

To determine whether intensive daily exercise had indeed resulted in ischemic damage in ΔH2–R19 transgenic mouse muscle, we analyzed muscle histology at the end of the eighth day of exercise (Figure 7, B and C, and Supplemental Figure 10). Muscles from ΔH2–R15 transgenic mice appeared healthy, with occasionally centrally nucleated myofiber (<1%) (Figure 7B and Supplemental Figure 10). In contrast, we observed frequent focal myofiber degeneration and regeneration in muscles obtained from ΔH2–R19 transgenic mice (Figure 7C and Supplemental Figure 10). Importantly, we also detected prominent macrophage infiltration in these loci (Figure 7C). Taken together, our data strongly suggest that restoring sarcolemmal nNOS can improve muscle perfusion, prevent ischemic damage in contracting muscle, and enhance exercise performance.

Discussion

nNOS plays a pivotal regulatory role in skeletal muscle physiology and disease (1). Interestingly, nNOS function depends on its location at the sarcolemma. Loss of sarcolemmal nNOS has been shown to induce functional ischemia and exaggerate exercise-associated fatigue (2, 3, 9, 10). For these reasons, there has been a great interest in understanding the mechanisms involved in anchoring nNOS to the sarcolemma.

Studies in the mid-1990s suggested that the correct positioning of nNOS requires the DGC, a multimeric protein complex consisting of dystrophin, dystroglycans, sarcoglycans, sarcospan, syntrophin, and dystrobrevin. Subsequent biochemical, structural, and genetic analyses demonstrated an essential role for syntrophin (7, 17–20). In particular, the PDZ domain of syntrophin forms a complex with the PDZ domain of nNOS (17, 18). At the same time, it was suggested that nNOS recruitment might require dystrophin. Since the dystrophin C-terminal domain contains a syntrophin binding site, the involvement of dystrophin seems quite logical. Surprisingly, sarcolemmal nNOS expression is not altered in *mdx* mice that express C-terminal domain–truncated dystrophins (15, 16). Furthermore, even in the presence of an intact C-terminal domain, nNOS is not detected at the sarcolemma (21, 25, 31). Taken together, these findings indicate that the dystrophin C-terminal domain may, at most, play a nominal role in nNOS recruitment.

A more puzzling issue is that nNOS is not always present on the sarcolemma even when syntrophin is there (16, 21, 23, 25). Apparently, additional help is needed to anchor nNOS to the sarcolemma. Several candidates have been proposed. These include other proteins in the DGC or other proteins that interact with the DGC, such as aquaporin-4, sodium channel, calcium pump, and caveolin-3 (32–34). Unfortunately, none of these have been confirmed.

Different regions in the dystrophin N-terminal and rod domains (such as exons 3–7 or 8, 10–42, 45, 45–47, and 51–52) have also been suggested to help recruit nNOS to the sarcolemma (21, 22, 35). Nevertheless, defining the nNOS recruiting domain in dystrophin has proven to be a quite challenging task. Several lines of

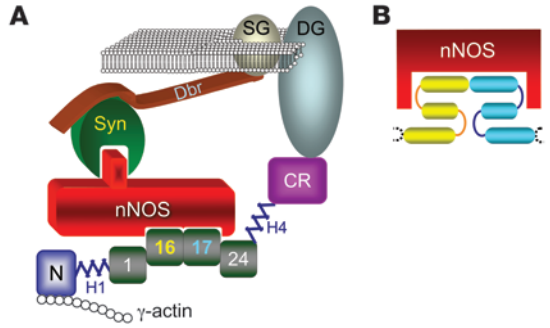

Figure 8
Schematic outline of sarcolemmal nNOS recruitment by an R16/17-containing microdystrophin gene. (**A**) The N-terminal domain (N) of the ΔR2–15/ΔR18–23/ΔC microgene interacts with γ-actin. The cysteine-rich domain (CR) of this microgene interacts with the dystroglycan complex (DG). Syntrophin (Syn) is brought to the sarcolemma by dystrobrevin (Dbr), which binds to the sarcoglycan complex (SG). nNOS recruitment requires 2 independent interactions, one between the nNOS PDZ β-finger and the syntrophin PDZ domain and the other between the nNOS PDZ groove and R16/17. Numbers denote spectrin-like repeats; H1 and H4, hinge 1 and hinge 4. (**B**) The hypothetical nNOS-R16/17 interaction model. The C-terminal helix of R16 joins the N-terminal helix of R17 to form a long helix. The R16/17 dimer then binds to the groove in the nNOS PDZ domain. Yellow, R16; blue, R17; dotted, flanking repeats.

evidence suggest that dystrophin may not bind to nNOS directly. First, it has been shown that nNOS interacts with other proteins mainly through the PDZ–PDZ domain interaction (36, 37). However, dystrophin does not contain a classic PDZ domain. Second, 2 independent studies have failed to detect a direct interaction between full-length dystrophin and nNOS (8, 21). Proving an indirect interaction is technically much more difficult. Third, it is not clear whether the dystrophin-nNOS interaction (assuming there is one) depends on a single defined region or several discontinuous regions in dystrophin.

In this study, we took a systemic approach to map the nNOS localization domain in dystrophin. We started with the ΔH2–R19 minigene (26). We have previously confirmed that this minigene cannot restore sarcolemmal nNOS (23, 25). Based on this information, we hypothesized that the H2-to-R19 region should contain the domain(s) required for nNOS recruiting. By in vivo plasmid transfection and AAV-mediated gene transfer, we narrowed down the nNOS recruiting domain to R16/17 (Figures 1 and 2, Supplemental Figures 2–4, and Table 1). We found that these 2 repeats were necessary to anchor nNOS to the sarcolemma. Furthermore, R16/17-mediated nNOS recruitment was not dependent on the flanking repeats or the dystrophin C-terminal domain. Interestingly, we also observed an interaction between the nNOS PDZ domain and R16/17, although its strength was lower than that of the interaction between the nNOS PDZ domain and the syntrophin PDZ domain (Figure 2, D and E). Based on these results, we here propose a novel nNOS recruitment model (Figure 8). According to this model, nNOS localization requires 2 independent interactions, one between R16/17 and the nNOS PDZ domain and the other between the syntrophin PDZ domain and the nNOS PDZ domain.

This model raises several interesting questions. First, how can a single nNOS PDZ domain interact with 2 partners at the same time? A ternary complex involving the nNOS PDZ domain has been demonstrated before (34). However, in this type of the complex, the nNOS PDZ domain only interacts with one partner (such as CAPON and postsynaptic density proteins). This intermediate partner then recruits the third partner to the complex (such as small G protein Dexras 1, synapsins, and NMDA receptor) (34). The classical PDZ domain consists of 2 α helices (αA and αB) and 6 β-sheets (from βA to βF). αB and βB form a groove for ligand binding (37). The nNOS PDZ domain includes the first 150 N-terminal residues of nNOS. Amino acids 1–100 express the classic groove structure for ligand binding. The next 30 residues form a unique β-finger (17, 18). Interestingly, the syntrophin PDZ domain only binds to the β-finger. This leaves the nNOS PDZ groove unoccupied (17, 18, 38). Thus, there is a structural basis for the nNOS PDZ domain to bind to both syntrophin and R16/17 simultaneously (38).

Second, R16/17 does not seem to be a good ligand for the nNOS PDZ groove. The short C-terminal peptide motif and the internal peptide motif are the classical ligands for the PDZ groove (37). Dystrophin does not carry these motifs. It is currently unclear how spectrin-like repeats may interact with the PDZ domain. Interestingly, such interaction has also been observed in another PDZ domain–containing protein. Xia et al. have demonstrated that the PDZ domain of the actinin-associated LIM protein binds to spectrin-like repeats in α-actinin-2 (39). Interestingly, this interaction also requires 2 complete repeats (39). Taking together, these findings reveal a new recognition mode for the PDZ domain. The PDZ domain is one of the most frequently used scaffolding modules. Approximately 400 PDZ domains have been identified in the human genome. The identification/confirmation of spectrin-like repeats as a PDZ domain ligand sheds new light on our understanding of protein-protein interaction and oligomerization.

R16/17 is encoded by exons 41–46 (40). This explains the findings seen in the majority of the clinical cases. In these patients, the loss of sarcolemmal nNOS correlates with mutations between exons 41 and 46 (21, 22, 35). However, sarcolemmal nNOS is also missing in some patients who were reported to carry mutations in other regions of the dystrophin gene, such as exons 3–8 and 48–52 (21, 22, 35). There are at least 2 possibilities. Spectrin-like repeats are modular repeating elements. Each repeat is composed of 3 α-helices linked by turns (41). However, the structural unit of the dystrophin rod domain is not based on individual repeats. Instead, it is believed that the biophysical unit is formed by adjacent repeats in a nested manner (Figure 8B) (42). Disruption of one repeat may alter structural conformation of the nearby units and influence the correct phasing of the entire rod domain (43). Hence, mutations in other exons may alter the noncanonical PDZ groove binding motif formed by R16/17. Alternatively, it is also possible that these patients carry additional small mutations (such as single nucleotide change) between exons 41 and 46.

The ultimate goal of our study is to develop an effective gene therapy to treat all affected muscles in DMD/BMD. AAV is the only viral vector proven to be capable of body-wide gene delivery (27, 44). However, AAV cannot carry the full-length dystrophin coding sequence. Minimizing the dystrophin gene offers a valid avenue to circumvent this problem (26). A variety of different minigenes and microgenes have been developed. Unfortunately, none of the abbreviated genes have been conclusively shown to recruit nNOS to the sarcolemma.

Based on the finding that R16/17 is sufficient to restore sarcolemmal nNOS, we generated a new microdystrophin gene,

ΔR2–15/ΔR18–23/ΔC. This microgene is similar to our previously reported ΔR4–23/ΔC microgene, except that R2–H2 is replaced by R16/17 (Figure 2A) (16, 26). Local and systemic gene transfer studies were performed in newborn and adult mouse DMD models. In *mdx*, *mdx4cv*, and MyoD/dystrophin double-knockout mice, the R16/17-containing microgene not only restored sarcolemmal nNOS, but also effectively reduced muscle histopathology and enhanced sarcolemma integrity (Figure 2, Figure 3, and Supplemental Figures 4 and 5). Furthermore, muscle strength and resistance to contraction-induced injury were improved to levels comparable to those resulting from ΔR4–23/ΔC microgene treatment (Figure 3B and Supplemental Figure 6).

One caveat with the microgenes is the uncertainty of their function in the canine animal model and human patients (45). On the other hand, the minigenes are derived from a remarkably functional template isolated from a patient with very mild BMD (46). They also restore muscle-specific forces to normal levels (Figure 4D) (26). Importantly, the minigenes can be delivered by *trans*-splicing AAV vectors to all muscles in the body (25, 28). From this standpoint, minigene therapy could be more effective than microgene therapy. To determine the therapeutic advantage of the R16/17-containing minigene, we next compared muscle force, femoral artery hemodynamics, muscle perfusion, and treadmill running in ΔH2–R15 and ΔH2–R19 transgenic mice (Figures 4–7 and Supplemental Figures 7, 8, and 10). Both transgenic strains were able to recover wild-type-level muscle force (Figure 4D). However, only the R16/17-containing minigene transgenic mice (ΔH2–R15) showed significantly improved perfusion in contracting muscle (Figure 5, Figure 6, and Supplemental Figure 8). Furthermore, restoring sarcolemmal nNOS by transfection of the ΔH2–R15 minigene significantly enhanced exercise performance and prevented ischemic damage (Figure 7 and Supplemental Figure 10).

Taken together, our studies provide evidence that R16/17 is essential for anchoring nNOS to the sarcolemma. The R16/17-containing mini-/microgenes may be more effective for DMD gene therapy than all previously described mini-/microgenes. Our findings also shed new light on the molecular mechanisms of nNOS PDZ domain–mediated scaffolding. Future studies on how R16/17 coordinates with syntrophin to bring nNOS to the sarcolemma may unravel yet-unrecognized aspects of this fascinating biological process.

Methods

Mini- and microdystrophin gene construction. All the minigenes and microgenes were derived from the human dystrophin gene. Standard molecular cloning techniques were used to generate synthetic dystrophin genes (47). Final products were confirmed by sequencing the junction sites and by restriction analysis. Transcriptional regulation was under the control of the CMV promoter and the SV40 polyA signal.

Immunofluorescence and immunohistochemistry staining. Dystrophin was detected with a series of epitope-specific antibodies (Supplemental Table 1). Dys-1, -2, and -3 (Novocastra) recognize R6–8, the C-terminal domain, and human dystrophin H1, respectively. Mandys 8 (Sigma-Aldrich) recognizes R11. Mandys 102 (a gift from Glenn Morris and Lam Le, The Robert Jones and Agnes Hunt Orthopaedic Hospital, Oswestry, United Kingdom) recognizes R16. Manex 44A, 46B, and 50 recognize R17, R18, and H3, respectively (from Glenn Morris and Lam Le) (48). nNOS was detected with a polyclonal antibody (1:2,000; Santa Cruz Biotechnology Inc.). Immunofluorescence staining was performed by using a previously published protocol (25). Immunohistochemistry staining was performed by using the VECTASTAIN ABC kit (Vector Laboratories). Macrophages were detected with the rat anti-mouse monoclonal antibody F4/80 (1:200; Caltag Laboratories, Invitrogen).

In situ nNOS activity staining. Histochemical evaluation of nNOS activity was performed according to a published protocol (49). nNOS appears as blue staining under the bright field.

Yeast two-hybrid assay. Yeast two-hybrid assay was performed with the Matchmaker GAL4 Two-Hybrid System 3 (Clontech). The syntrophin plasmid was a gift from Stanley C. Froehner and Marvin Adams (University of Washington, Seattle, Washington, USA) (20). The nNOS plasmid was a gift from David Bredt (UCSF, San Francisco, California, USA) and Samie R. Jaffrey (Cornell University Weill Medical College, New York, New York, USA) (7). All constructs were sequenced prior to use. The dot assay (Figure 2D) was performed on leucine/tryptophan/histidine triple-deficient medium. For quantitative interaction assay (Figure 2E), β-galactosidase activity was measured using the Galacto-Light system (Applied Biosystems).

Mouse models for DMD. All animal experiments were approved by the Animal Care and Use Committee of the University of Missouri or the UT Southwestern Medical Center and were in accordance with NIH guidelines. All experimental mice were housed in a specific pathogen–free facility. Three dystrophin-deficient mouse models were used, including the naturally occurring *mdx* mice, chemically induced *mdx4cv* mice, and MyoD/dystrophin double-knockout mice. *mdx* and *mdx4cv* mice are on the BL10 and C57BL/6 backgrounds, respectively (50, 51). These mice were purchased from The Jackson Laboratory. The breeding pair of MyoD/dystrophin double-knockout mice was a gift from Michael Rudnicki (Ottawa Health Research Institute, Ottawa, Ontario, Canada) (29). These mice were maintained on the 129/BL10 background. Male mice were used in all studies.

Transgenic mice. The skeletal-specific transgenic mice were generated at the University of Missouri Transgenic Animal Core. Synthetic human dystrophin genes were expressed under the transcriptional regulation of the human skeletal α-actin promoter and bovine growth hormone (26). The founder mice were backcrossed with *mdx4cv* and *mdx* mice for 3 and 5 generations, respectively, before being used in the study.

AAV infection. Recombinant AAV-6 and AAV-9 vectors were generated according to previously published protocols (25, 28). Local injection was performed with AAV-6 on the TA muscle (6×10^{10} viral genome [vg] particles, 50-day-old *mdx* mice) and the gastrocnemius muscle (1×10^{11} vg particles, 2-month-old *mdx* mice). Systemic injection was performed with AAV-9 in neonatal *mdx* and *mdx4cv* mice (facial vein injection, 1×10^{12} vg particles/mouse) and in 2-month-old MyoD/dystrophin double-knockout mice (tail vein injection, 5.5×10^{12} vg particles/mouse).

Western blot analysis. Whole muscle lysate was extracted from the TA muscle, and Western blot analysis was performed according to a previously published protocol (52). Membrane-enriched microsomal preparations were produced using the quadriceps femoris muscle according to a previously described protocol (53). Dystrophin was detected with an antibody against the C-terminal domain of dystrophin (Dys-2, 1:100; Novocastra). nNOS was detected with a rabbit anti-nNOS polyclonal antibody (1:4,000; Upstate, Millipore). Utrophin was detected with a mouse monoclonal antibody (1:250; BD). GAPDH (1:3,000; Upstate) was used as a loading control in whole muscle lysate Western blot analysis. α-Sarcoglycan was detected with a mouse monoclonal antibody (1:1,000; Vector Laboratories). Dystrobrevin was revealed with a mouse monoclonal antibody (1:1,000; BD).

Hemodynamic measurements. Femoral vascular conductance in anesthetized male transgenic *mdx* (6- to 20-month-old) and *mdx4cv* (6- to 11-month-old) mice was measured using a VF-1 pulsed Doppler velocimeter (model HVPD-20; Crystal Biotech) according to our previous publication (2). Conductance responses to intraarterial hind limb injection of the α-adrenergic vasoconstrictor norepinephrine were measured in resting and contracting muscles (by stimulating sciatic nerve using trains of pulses at 100 Hz; model S88,

Grass Technologies) in intact animals as previously described (2). In transgenic *mdx* mice, 2 doses of norepinephrine were applied (in a total volume of 2–10 μl; first dose, 4.2 ± 0.4 ng; second dose, 7.6 ± 0.8 ng). In transgenic *mdx4cv* mice, 1 dose of norepinephrine was used (4–10 ng in 2–5 μl). Femoral vascular conductance responses to norepinephrine were calculated by integrating the area under the response curve (AUC).

Microsphere blood flow measurement. Tissue blood flow in resting and exercising mice was measured in 13- to 15-month-old male transgenic *mdx* mice (n = 12 for ΔH2–R15, n = 8 for ΔH2–R19) according to our previously published protocol (54). The investigator was blinded to the mouse genotype. Prior to the study, experimental mice were acclimated to a 15° uphill treadmill for at least 4 days. Mice were anesthetized with 1.5% isoflurane inhalation. Under the anesthesia, a 0.5-cm skin incision was made, and the left carotid artery was dissected free of connective tissue. A PE50 catheter with tapered tip was inserted into the artery under a ×20 dissecting microscope. Through a subcutaneous tunnel, the catheter was exteriorized at the back of the neck. After the skin incision was closed, ^{85}Sr-labeled microspheres (about 1,500,000 cpm; PerkinElmer) were infused into the anesthetized mouse in 0.2-ml volume (0.1 ml microsphere plus 0.1 ml animal blood). At least 3 hours after mice recovered from anesthesia, mice were allowed to run on the 15° uphill treadmill for 1 minute at a speed of 15 m/min. ^{141}Ce-labeled microspheres (about 1,500,000 cpm; PerkinElmer) were infused into the mice over 20 seconds while they were running on the treadmill. After ^{141}Ce-labeled microsphere infusion, mice were sacrificed. All tissues from each mouse were dissected, and radioactivity in each tissue was counted in a Wallac Wizard 1480 Autogamma Counter. The reading was corrected for spillover of the isotopes between counting windows as we described previously (54). Proper microsphere distribution was verified by detection of similar levels of radioactivity in the left and right kidneys. Final tissue blood flow in each muscle (or organ) was calculated using the following formula: tissue blood flow (ml/min/100 g) = (cardiac output, ml/min) × (fraction of total radioactivity in the tissue)/(tissue weight, g) × 100. The cardiac output at resting and during exercise is 20 ml/min and 30 ml/min, respectively (55, 56). The fraction of total radioactivity in the tissue was calculated using the following formula: (measured radioactivity in the tissue, cpm)/(total radioactivity injected into the animal, cpm). Five mice died during surgery (n = 4 for ΔH2–R15, n = 1 for ΔH2–R19), and 2 mice with poor microsphere distribution (based on left and right kidney blood flow; n = 1 for each mouse strain) were excluded from the analysis.

Treadmill. Uphill (7°) treadmill experiments were performed using an Exer-3/6 open treadmill (Columbus Instruments). Six-month-old male mice were acclimated to treadmill during a 5-day training session. After training, mice were subjected to treadmill exercise for 8 continuous days, and running distance was recorded every day for each mouse. The exact same protocol was used for every mouse, irrespective of the strain. After the last treadmill running, mice were euthanized, and limb muscles were collected for morphology studies.

Statistics. Data are presented as mean ± SEM. Statistical analysis was performed with SPSS software. Statistical significance for multiple group comparison was determined by 1-way ANOVA followed by Tukey's post hoc analysis. Two-tailed (or paired, when appropriate) t test was used for 2-group comparison. Difference was considered significant when P was less than 0.05.

Acknowledgments

We thank Glenn Morris, Lam Le, Stanley Froehner, Marvin Adams, David Bredt, Samie Jaffrey, and Michael Rudnicki for providing experiment reagents. We thank Elizabeth Critser and Natalia Karasseva for help with generating the founder transgenic mice. We thank John Cannon, Deyu Fang, and Harold Laughlin for helpful discussion. This work was supported by grants from the NIH (AR49419, AR57209, NS62934, and HL37387 to D. Duan, J.S. Chamberlain, G.D. Thomas, H.T. Yang, R.L. Terjung) and the Muscular Dystrophy Association (to D. Duan and J.S. Chamberlain).

Received for publication June 27, 2008, and accepted in revised form January 7, 2009.

Address correspondence to: Dongsheng Duan, Department of Molecular Microbiology and Immunology, University of Missouri, One Hospital Dr., Columbia, Missouri 65212, USA. Phone: (573) 884-9584; Fax: (573) 882-4287; E-mail: duand@missouri.edu.

1. Stamler, J.S., and Meissner, G. 2001. Physiology of nitric oxide in skeletal muscle. *Physiol. Rev.* **81**:209–237.
2. Thomas, G.D., et al. 1998. Impaired metabolic modulation of alpha-adrenergic vasoconstriction in dystrophin-deficient skeletal muscle. *Proc. Natl. Acad. Sci. U. S. A.* **95**:15090–15095.
3. Sander, M., et al. 2000. Functional muscle ischemia in neuronal nitric oxide synthase-deficient skeletal muscle of children with Duchenne muscular dystrophy. *Proc. Natl. Acad. Sci. U. S. A.* **97**:13818–13823.
4. Kunkel, L.M. 2005. 2004 William Allan Award address. Cloning of the DMD gene. *Am. J. Hum. Genet.* **76**:205–214.
5. Mendell, J.R., Engel, W.K., and Derrer, E.C. 1971. Duchenne muscular dystrophy: functional ischemia reproduces its characteristic lesions. *Science.* **172**:1143–1145.
6. Parker, J.M., and Mendell, J.R. 1974. Proximal myopathy induced by 5-HT-imipramine simulates Duchenne dystrophy. *Nature.* **247**:103–104.
7. Brenman, J.E., Chao, D.S., Xia, H., Aldape, K., and Bredt, D.S. 1995. Nitric oxide synthase complexed with dystrophin and absent from skeletal muscle sarcolemma in Duchenne muscular dystrophy. *Cell.* **82**:743–752.
8. Chang, W.J., et al. 1996. Neuronal nitric oxide synthase and dystrophin-deficient muscular dystrophy. *Proc. Natl. Acad. Sci. U. S. A.* **93**:9142–9147.
9. Percival, J.M., et al. 2008. Functional deficits in nNOSmu-deficient skeletal muscle: myopathy in nNOS knockout mice. *PLoS ONE.* **3**:e3387.
10. Kobayashi, Y.M., et al. 2008. Sarcolemma-localized nNOS is required to maintain activity after mild exercise. *Nature.* **456**:511–515.
11. Ahn, A.H., and Kunkel, L.M. 1995. Syntrophin binds to an alternatively spliced exon of dystrophin. *J. Cell Biol.* **128**:363–371.
12. Suzuki, A., Yoshida, M., and Ozawa, E. 1995. Mammalian alpha 1- and beta 1-syntrophin bind to the alternative splice- prone region of the dystrophin COOH terminus. *J. Cell Biol.* **128**:373–381.
13. Yang, B., Jung, D., Rafael, J.A., Chamberlain, J.S., and Campbell, K.P. 1995. Identification of alpha-syntrophin binding to syntrophin triplet, dystrophin, and utrophin. *J. Biol. Chem.* **270**:4975–4978.
14. Yoshida, M., et al. 2000. Biochemical evidence for association of dystrobrevin with the sarcoglycan-sarcospan complex as a basis for understanding sarcoglycanopathy. *Hum. Mol. Genet.* **9**:1033–1040.
15. Crawford, G.E., et al. 2000. Assembly of the dystrophin-associated protein complex does not require the dystrophin COOH-terminal domain. *J. Cell Biol.* **150**:1399–1410.
16. Yue, Y., Liu, M., and Duan, D. 2006. C-terminal truncated microdystrophin recruits dystrobrevin and syntrophin to the dystrophin-associated glycoprotein complex and reduces muscular dystrophy in symptomatic utrophin/dystrophin double knock-out mice. *Mol. Ther.* **14**:79–87.
17. Hillier, B.J., et al. 1999. Unexpected modes of PDZ domain scaffolding revealed by structure of nNOS-syntrophin complex. *Science.* **284**:812–815.
18. Tochio, H., Zhang, Q., Mandal, P., Li, M., and Zhang, M. 1999. Solution structure of the extended neuronal nitric oxide synthase PDZ domain complexed with an associated peptide. *Nat. Struct. Biol.* **6**:417–421.
19. Kameya, S., et al. 1999. alpha1-syntrophin gene disruption results in the absence of neuronal- type nitric-oxide synthase at the sarcolemma but does not induce muscle degeneration. *J. Biol. Chem.* **274**:2193–2200.
20. Adams, M.E., Mueller, H.A., and Froehner, S.C. 2001. In vivo requirement of the alpha-syntrophin PDZ domain for the sarcolemmal localization of nNOS and aquaporin-4. *J. Cell Biol.* **155**:113–122.
21. Chao, D.S., et al. 1996. Selective loss of sarcolemmal nitric oxide synthase in Becker muscular dystrophy. *J. Exp. Med.* **184**:609–618.
22. Wells, K.E., et al. 2003. Relocalization of neuronal nitric oxide synthase (nNOS) as a marker for complete restoration of the dystrophin associated protein complex in skeletal muscle. *Neuromuscul. Disord.* **13**:21–31.
23. Judge, L.M., Haraguchi, M., and Chamberlain, J.S. 2006. Dissecting the signaling and mechanical functions of the dystrophin-glycoprotein complex. *J. Cell Sci.* **119**:1537–1546.
24. Grady, R.M., et al. 1999. Role for alpha-dystrobrevin

in the pathogenesis of dystrophin-dependent muscular dystrophies. *Nat. Cell Biol.* **1**:215–220.
25. Lai, Y., et al. 2005. Efficient in vivo gene expression by trans-splicing adeno-associated viral vectors. *Nat. Biotechnol.* **23**:1435–1439.
26. Harper, S.Q., et al. 2002. Modular flexibility of dystrophin: implications for gene therapy of Duchenne muscular dystrophy. *Nat. Med.* **8**:253–261.
27. Gregorevic, P., et al. 2004. Systemic delivery of genes to striated muscles using adeno-associated viral vectors. *Nat. Med.* **10**:828–834.
28. Ghosh, A., Yue, Y., Long, C., Bostick, B., and Duan, D. 2007. Efficient whole-body transduction with trans-splicing adeno-associated viral vectors. *Mol. Ther.* **15**:750–755.
29. Megeney, L.A., Kablar, B., Garrett, K., Anderson, J.E., and Rudnicki, M.A. 1996. MyoD is required for myogenic stem cell function in adult skeletal muscle. *Genes Dev.* **10**:1173–1183.
30. Dudley, R.W., et al. 2006. Sarcolemmal damage in dystrophin deficiency is modulated by synergistic interactions between mechanical and oxidative/nitrosative stresses. *Am. J. Pathol.* **168**:1276–1287.
31. Li, S., et al. 2006. A highly functional mini-dystrophin/GFP fusion gene for cell and gene therapy studies of Duchenne muscular dystrophy. *Hum. Mol. Genet.* **15**:1610–1622.
32. Miyagoe-Suzuki, Y., and Takeda, S.I. 2001. Association of neuronal nitric oxide synthase (nNOS) with alpha1-syntrophin at the sarcolemma. *Microsc. Res. Tech.* **55**:164–170.
33. Albrecht, D.E., and Froehner, S.C. 2002. Syntrophins and dystrobrevins: defining the dystrophin scaffold at synapses. *Neurosignals.* **11**:123–129.
34. Kone, B.C., Kuncewicz, T., Zhang, W., and Yu, Z.Y. 2003. Protein interactions with nitric oxide synthases: controlling the right time, the right place, and the right amount of nitric oxide. *Am. J. Physiol. Renal Physiol.* **285**:F178–F190.
35. Torelli, S., et al. 2004. Absence of neuronal nitric oxide synthase (nNOS) as a pathological marker for the diagnosis of Becker muscular dystrophy with rod domain deletions. *Neuropathol. Appl. Neurobiol.* **30**:540–545.
36. Kone, B.C. 2000. Protein-protein interactions controlling nitric oxide synthases. *Acta Physiol. Scand.* **168**:27–31.
37. Harris, B.Z., and Lim, W.A. 2001. Mechanism and role of PDZ domains in signaling complex assembly. *J. Cell. Sci.* **114**:3219–3231.
38. Abdelmoity, A., Padre, R.C., Burzynski, K.E., Stull, J.T., and Lau, K.S. 2000. Neuronal nitric oxide synthase localizes through multiple structural motifs to the sarcolemma in mouse myotubes. *FEBS Lett.* **482**:65–70.
39. Xia, H., Winokur, S.T., Kuo, W.L., Altherr, M.R., and Bredt, D.S. 1997. Actinin-associated LIM protein: identification of a domain interaction between PDZ and spectrin-like repeat motifs. *J. Cell Biol.* **139**:507–515.
40. Roberts, R.G., Coffey, A.J., Bobrow, M., and Bentley, D.R. 1993. Exon structure of the human dystrophin gene. *Genomics.* **16**:536–538.
41. Djinovic-Carugo, K., Young, P., Gautel, M., and Saraste, M. 1999. Structure of the alpha-actinin rod: molecular basis for cross-linking of actin filaments. *Cell.* **98**:537–546.
42. Calvert, R., Kahana, E., and Gratzer, W.B. 1996. Stability of the dystrophin rod domain fold: evidence for nested repeating units. *Biophys. J.* **71**:1605–1610.
43. Menhart, N. 2006. Hybrid spectrin type repeats produced by exon-skipping in dystrophin. *Biochim. Biophys. Acta.* **1764**:993–999.
44. Yue, Y., et al. 2008. A single intravenous injection of adeno-associated virus serotype-9 leads to whole body skeletal muscle transduction in dogs. *Mol. Ther.* **16**:1944–1952.
45. Sampaolesi, M., et al. 2006. Mesoangioblast stem cells ameliorate muscle function in dystrophic dogs. *Nature.* **444**:574–579.
46. England, S.B., et al. 1990. Very mild muscular dystrophy associated with the deletion of 46% of dystrophin. *Nature.* **343**:180–182.
47 Ausubel, F.M., et al., editors. 1995. *Current protocols in molecular biology*. John Wiley and Sons. New York, New York, USA.
48. Thanh, L.T., Nguyen, T.M., Helliwell, T.R., and Morris, G.E. 1995. Characterization of revertant muscle fibers in Duchenne muscular dystrophy, using exon-specific monoclonal antibodies against dystrophin. *Am. J. Hum. Genet.* **56**:725–731.
49. Hope, B.T., Michael, G.J., Knigge, K.M., and Vincent, S.R. 1991. Neuronal NADPH diaphorase is a nitric oxide synthase. *Proc. Natl. Acad. Sci. U. S. A.* **88**:2811–2814.
50. Bulfield, G., Siller, W.G., Wight, P.A., and Moore, K.J. 1984. X chromosome-linked muscular dystrophy (mdx) in the mouse. *Proc. Natl. Acad. Sci. U. S. A.* **81**:1189–1192.
51. Chapman, V.M., Miller, D.R., Armstrong, D., and Caskey, C.T. 1989. Recovery of induced mutations for X chromosome-linked muscular dystrophy in mice. *Proc. Natl. Acad. Sci. U. S. A.* **86**:1292–1296.
52. Li, D., Yue, Y., and Duan, D. 2008. Preservation of muscle force in mdx3cv mice correlates with low-level expression of a near full-length dystrophin protein. *Am. J. Pathol.* **172**:1332–1341.
53. Ervasti, J.M., and Campbell, K.P. 1991. Membrane organization of the dystrophin-glycoprotein complex. *Cell.* **66**:1121–1131.
54. Yang, H.T., Dinn, R.F., and Terjung, R.L. 1990. Training increases muscle blood flow in rats with peripheral arterial insufficiency. *J. Appl. Physiol.* **69**:1353–1359.
55. Flaim, S.F., and Zelis, R.F. 1980. Regional distribution of cardiac output in conscious rats at rest and during exercise. Effects of diltiazem. *Chest.* **78**:187–192.
56. Janssen, B., Debets, J., Leenders, P., and Smits, J. 2002. Chronic measurement of cardiac output in conscious mice. *Am. J. Physiol. Regul. Integr. Comp. Physiol.* **282**:R928–R935.